Immobilization of inorganic ion-exchanger into biopolymer foams - Application to cesium sorption

Chloe Vincent, Audrey Hertz, Thierry Vincent, Yves Barré, Eric Guibal

Immobilization of inorganic ion-exchanger into biopolymer foams – Application to cesium sorption

Chloë Vincent [a], Audrey Hertz [a], Thierry Vincent [b], Yves Barré [a], Eric Guibal [b,*]

[a] CEA Marcoule, DEN/DTCD/SPDE/LPSD, BP 17171, F-30207 Bagnols sur Cèze, France
[b] Ecole des Mines d'Alès, Centre des Matériaux des Mines d'Alès, C2MA/MPA/BCI, 6 avenue de Clavières, F-30319 Alès cedex, France

GRAPHICAL ABSTRACT

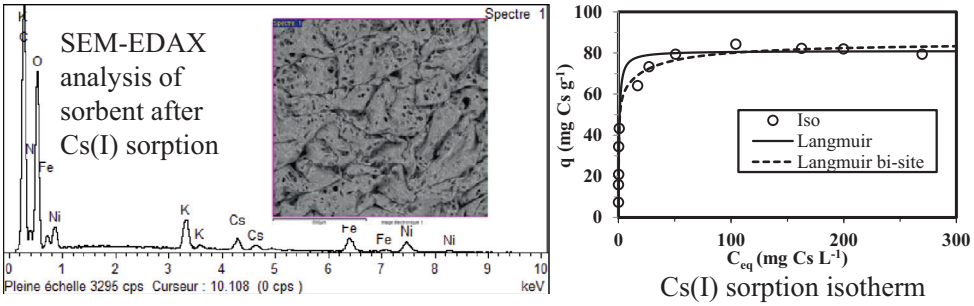

ABSTRACT

Nickel–potassium ferrocyanide (along with other ferrocyanide sub-products, as shown by mineralization, SEM–EDX and XRD analyses) has been immobilized in highly porous discs of chitin for the sorption of Cs(I) from near neutral solutions. The immobilization process allows synthesizing stable materials that can bind up to 80 mg Cs g^{-1} (i.e., 240 mg Cs g^{-1} ion-exchanger). Cesium sorption is hardly affected by the pH between pH 2 and 8. The sorbent is selective to Cs(I) even in the presence of high concentrations of Na(I), K(I), Rb(I) or NH_4^+. The pseudo-second order rate equation fits well kinetic profiles: the rate coef-ficient increases with the flow rate of recirculation (to force the access to potentially non-interconnected pores), as an evidence of the control of uptake kinetics by diffusion properties. In fixed-bed columns, the breakthrough curve is accurately described by the Clark model and the sorption capacity (at sorbent sat-uration) is consistent with the values obtained in sorption isotherms. Preliminary tests performed on ^{137}Cs spiked solutions confirm the efficiency of the material for the treatment of effluents bearing radionuclides.

Keywords:
Nickel–potassium ferrocyanide
Chitin
Highly porous discs
Sorption isotherms
Uptake kinetics
Breakthrough curves

1. Introduction

Nuclear energy contributes in many countries, including France, as an important power source. The safety control of this industrial sector is a key parameter for its development, not only in its normal operative conditions but also in the case of incident, or emergency. Recently, the Fukushima accident illustrated the necessity of developing appropriate processes for the recovery of radionuclides from accidental discharge. There are also specific needs for the development of new processes for the recovery and/or separation of radionuclides from highly saline solutions in normal operative conditions; for example in the life cycle (re-treatment) of the nuclear combustible where a number of radioelements are produced during fission reactions.

* Corresponding author. Tel.: +33 (0)466782734; fax: +33 (0)466782701.
E-mail address: Eric.Guibal@mines-ales.fr (E. Guibal).

At Fukushima, a large amount of radionuclides were released into water, soil and air. Among radionuclides, ^{137}Cs is considered the most abundant and hazardous due to diverse sources and relatively long half-life. As a result, numerous efforts have been undertaken to find effective and low cost methods to remove cesium from waste solutions.

Cesium recovery is generally operated using inorganic ion-exchangers such as ferrocyanides derivatives (including Prussian Blue) [1–8], zirconium phosphate [9–11], titanium phosphate [10], titanium dioxide [12] and ammonium molybdophosphate [13]. The main disadvantage of these materials is the size and the dispersion of these micro-particles that require appropriate solid/liquid separation techniques for recovering spent sorbents. Their application in fixed-bed columns is almost impossible due to clogging, and head pressure loss. For these reasons these inorganic ion-exchangers are generally functionalized by deposition/grafting on appropriate supports or encapsulation in specific materials, such as mineral oxide [14–17] or zeolite [18] supports, carbon fibrous materials [19,20], biosorbent [21], polymers [22–25] and biopolymers [26]. The challenge is combining the retention/confinement of the inorganic ion-exchanger and the optimization of mass transfer properties. Indeed, the immobilization of the inorganic ion-exchanger in a matrix may contribute to strongly increase the resistance to mass transfer (especially intraparticle diffusion). Biopolymers have recently retained great attention for the immobilization and encapsulation of a number of mineral sorbents [27], ion-exchangers [26,28–31], liquid extractants [33,33] or ionic liquids [35]. Their encapsulating properties are used for the synthesis of spherical resins or hybrid sorbents. Alginate and chitosan are two polysaccharides (renewable resources) that were extensively tested for the last decade for the elaboration of new supports based on their physical versatility: indeed, these biopolymers can be readily conditioned under different forms such as beads, membranes, fibers, tubes and scaffolds (foams and sponges).

Different systems based on chitosan or alginate have been investigated for elaborating hybrid foams (combining biopolymers and ionic liquids or inorganic ion-exchangers) to (a) bind metal anions [36], (b) prepare supported catalysts under the form of spherical resins [37], discs [38] and cylindrical foams [37,38]. The same procedure was used for the immobilization of nickel potassium hexacyanoferrate ion-exchanger in a chitin-based matrix (conditioned under the form of highly porous discs) for the binding of Cs(I) form acidic or neutral solutions (See Additional Material Section, Fig. AM1). Due to the partial solubility of chitosan is acidic solutions the reacetylation of the biopolymer was operated on the discs (containing the inorganic ion-exchanger) to improve the chemical stability of the hybrid material. The hybrid discs were immobilized in a filtration membrane holder and they were tested in a static mode with recirculation of the solution through the membrane (See Additional Material Section, Fig. AM2 for the description of operating system). The sorption properties of the material were tested in a first step on synthetic inactive solutions of Cs(I) through the study of pH effect, the impact of competitor ions, the investigation of uptake kinetics (considering the impact of recirculation flow rate, in order to evaluate the contribution of mass transfer properties), and sorption isotherms. The sorption of Cs(I) is also tested in fixed-bed columns (dynamic mode) and the stability of the sorbent is evaluated through (a) the quantification of nickel and iron release in the sorption mode, and (b) a first attempt to desorb Cs(I). Finally, the decontamination factor was evaluated on saline solutions spiked with ^{137}Cs. SEM and SEM–EDX analyses have also been carried out in order to characterize the materials (morphology and structure of the hybrid foams, distribution of elements before and after Cs(I) sorption).

2. Materials and methods

2.1. Materials

Potassium ferrocyanide ($K_4[Fe(CN)_6]\cdot 3H_2O$, Riedel-de Haën), nickel sulfate ($NiSO_4\cdot 6H_2O$, Chem-Lab), acetic anhydride ($C_4H_6O_3$, Sigma–Aldrich) were supplied as reagent grade products. Acetic acid (80% w/w, Carlo Erba), ethanol (96% w/w, Sodipro) were technical products. Chitosan (molecular weight 125,000 g mol^{-1}, deacetylation degree: 87%) was supplied by Aber-Technologies (France). Cesium nitrate was purchased from Merck AG (Germany).

2.2. Synthesis of sorbent

The synthesis of the potassium-nickel ferrocyanide ($K_2Ni[Fe(CN)_6]$) was prepared by reaction of two precursors, potassium ferrocyanide (9.0672 g, 0.0215 mole) and nickel sulfate (7.25 g, 0.0276 mole), in 500 mL of demineralized water under strong agitation for 30 min. The precipitate was recovered by centrifugation (for 5 min at 9000 rpm). The solid was re-suspended in 500 mL of demineralized water together with 15 g of chitosan. The suspension was maintained in strong agitation for 15 min before adding dropwise 15 mL of acetic acid. The suspension was maintained in strong agitation for 90 min; this agitation time is sufficient for achieving the complete dissolution of the biopolymer.

The second step in the process consisted in conditioning the material as highly porous foams. The mixture was poured in Petri dishes (using 18 g of the homogeneous suspension in 15 cm-diameter Petri dishes) before being frozen at −80 °C for 90 min. The water being frozen formed a porous network in the frozen discs. By freeze-drying water was sublimated and the porous network was maintained in the discs.

The third step consisted in the reacetylation of amine groups using acetic anhydride. The reacetylation may contribute to increase the chemical stability of the biopolymer, especially in terms of pH range. Chitosan being soluble in acidic solutions, the reacetylation of glucosamine moieties to acetylglucosamine (to form chitin) will offer the possibility to use the material also in acidic solution. For the reacetylation of chitosan, 5 g (dry) of the material was maintained in a mixture of ethanol (800 mL) and acetic anhydride (200 mL) under reflux.

The last step consisted in the careful rinsing of the materials (to remove traces of acetic anhydride that did not react, and other possible impurities), followed by a final freeze-drying.

2.3. Characterization of sorbent

2.3.1. SEM and SEM–EDX analysis

The morphology and the distribution of inorganic ion-exchanger and Cs element in the materials were determined with a Scanning Electron Microscope coupled with Energy Dispersive X-ray analysis (SEM–EDX). SEM observations were performed using an Environmental Scanning Electron Microscope (ESEM) Quanta FEG 200, equipped with an OXFORD Inca 350 Energy Dispersive X-ray microanalysis (EDX) system. The use of environmental SEM allowed the direct observations of materials, without previous metallization of the samples. The topography of the samples was observed using secondary electron flux while the backscattered electrons were used for the identification and localization of heavy metals at the surface of the materials (by phase contrast). SEM–EDX facilities were used for the detection of elements and their semi-quantitative analysis (Cs and principal elements representative of the inorganic ion-exchanger; i.e., Fe, K and Ni elements).

2.3.2. XRD analysis

X-ray diffraction (XRD) data (on powders) were collected using a BRUKER Advance D8 diffractometer in a θ–θ configuration employing the Cu Kα radiation (λ = 1.54 Å) with a fixed divergence slit size 0.3° and a rotating sample stage. The samples were scanned between 10° and 70° with the VANTEC-1 detector. The qualitative analysis was performed with the X'Pert High Score Plus software (version 2.1).

2.3.3. Material mineralization

Wet mineralization of the materials was performed by reaction with a 18 M sulfuric acid solution at boiling temperature followed by successive additions of 1 mL volumes of hydrogen peroxide (30% v/v), till complete discoloration. The solutions were then analyzed for Fe, Ni and K analysis using an ICP-AES Activa M (Jobin-Yvon, inductively coupled plasma atomic emission spectrometer).

2.4. Sorption experiments

The wide porosity of the materials (air bubbles blocked in the internal porosity) and the heterogeneous interconnectivity of the channel network do not insure efficient contact of the solution with reactive internal structures. For these reasons it appears more efficient using the foams immobilized in filtration membrane holders and to circulate (under forced flux) the solutions through the membranes (See Additional Material Section, Fig. AM2). All experiments were performed at room temperature (20 ± 1 °C).

2.4.1. Static mode

Kinetic experiments were carried out using 1 disc (approximately 100 mg, immobilized in a filtration membrane holder; diameter: 25 mm) fed downflow by a peristaltic pump (at 300 mL min^{-1} flow rate) on a recirculation mode with 1 L of 10 mg Cs L^{-1} solution (pH 7). Samples were collected over 24 h of contact and analyzed using a Varian atomic absorbance spectrometer (AAS). A complementary experiment was performed in batch system using directly the potassium-nickel ferrocyanide powder in an agitated tank reactor collecting samples at the same times. The samples were filtered through a 1 µm membrane filter, before Cs(I) analysis by atomic absorption spectrometry (AAS, Varian AA 20 spectrometer).

Sorption isotherms were obtained using the same method: a series of discs (immobilized in individual filtration membrane holders, approximate mass: $m \approx 100$ mg) was fed downflow with a pump (flow rate 30 ml min^{-1}, superficial flow velocity: 3.7 m h^{-1}) with V = 50 mL (and with recirculation) cesium solutions at pH 7 with increasing concentrations of Cs(I) (i.e., C_0: 10–400 mg Cs(I) L^{-1}). Sodium nitrate was added to the solution (final concentration 0.01 M). Residual metal concentrations (C_{eq}, mg Cs L^{-1}) after 48 hours of contact were analyzed by AAS. The mass balance equation was applied for calculating the sorption capacity q (mg Cs g^{-1}) $q = (C_0 - C_{eq})V/m$.

The influence of the pH and of the presence of competitor ions was investigated using the same procedure. Solutions of Cs(I) (250 mg Cs(I) L^{-1}) with pH adjusted between 1 and 9 were pumped through a sorbent disc (flow rate: 30 ml min^{-1}). Residual concentrations and final pHs were measured after 48 h of contact for determining the sorption efficiency and the sorption capacity, together with the pH change during the sorption step. The competition of monovalent cations was also tested using the same procedure while adding increasing concentrations of sodium nitrate (0.01–1 M), potassium nitrate (0.01–0.1 M), ammonium nitrate (0.01–0.5 M) and rubidium nitrate (0.01–0.5 M).

2.4.2. Dynamic mode

The fixed-bed column was operated by pumping a 10 mg Cs L^{-1} solution (containing 0.01 M $NaNO_3$) through the column (filled with 5 discs; i.e., 0.5 g). The flow rate was set to 150 mL h^{-1} (i.e., superficial velocity: 0.3 m h^{-1}). A fraction collector was used to withdraw samples (which were further analyzed by AAS) at fixed times and the breakthrough curve was plotted.

2.4.3. ^{137}Cs sorption tests

Preliminary tests were performed on ^{137}Cs-spiked solutions (in 0.01 M $NaNO_3$ solutions) using the same procedure as for stable Cs. A disc (m: 94 mg) was immobilized in a membrane holder and 50 mL of metal solution was recirculated through the disc at a flow rate of 6 mL min^{-1} for 24 h. The ^{137}Cs load was constant and set at 41,000 Bq L^{-1}, while 3 increasing concentrations of stable Cs were added (i.e., C_0: 4×10^{-5}, 2×10^{-3} and 2×10^{-2} mmol L^{-1}). The same disc was used for the 3 successive tests. The gamma counting (Eurisys Mesure with a germanium detector) served to analyze the residual ^{137}Cs amount in the spiked solution. Assuming that both active and stable Cs were equally sorbed on the material, the counting of active Cs allowed determining the residual traces of stable Cs and calculating the sorption capacity (amount sorbed at each step and cumulative sorption capacity).

3. Results and discussion

3.1. Sorbent characterization

The high porosity of the materials was shown by scanning electron microscopy (Fig. 1) and it was confirmed by pycnometer characterization that showed that about 89% (±1.3%) of the volume of the material is porous. Though this technique is not very precise for this type of material it gives a first indication of the macroporous structure. The volumetric mass is about 1.67 (±0.04) g cm^{-3}. Fig. 1A shows that the material is characterized by a much opened structure with irregular holes/pores: 50–100 µm for the majority of these cavities/channels and some dispersed 150–200 µm channels. Fig. 1B shows at a higher magnitude that the surface of the biopolymer membrane is homogeneously covered by small particles (a few microns) of inorganic ion-exchanger particles. At a higher magnitude, Fig. 1C shows the details of agglomerated particles (few tens of nanometers) covering the whole surface of the material.

Fig. 2 shows the SEM–EDX analysis of the hybrid foams before and after Cs(I) sorption. The scanning electron micrograph shows the change in the structure of the material: the structure appeared more compact without the large channels that were initially observed in the raw material. This is probably due to the air-drying of the foam after metal sorption that makes more compact the opened structure of the biopolymer. The X-ray diffraction pattern allows identifying the constituents of the inorganic ion-exchanger (i.e., Fe, Ni and K) in the raw material and the presence of Cs element after metal sorption. A semi-qualitative analysis was also performed on these materials (Table 1). The Ni/Fe molar ratio is close to 1.2, while that of K/Fe is about 1.23. This means that the theoretical stoichiometry of metals is close to $K_{1.23}Ni_{1.2}[Fe(CN)_6]$. After Cs(I) sorption the atomic percentage of Cs elements is close to 0.47% while that of K(I) decreases by 0.3–0.4%; other metal elements of the inorganic ion-exchanger (i.e., Fe and Ni) are hardly changed (at least in regard of the sensitivity and accuracy of the SEM–EDX analysis). This observation confirms, as expected, that Cs(I) is exchanged with K(I).

After mineralization and quantification of elements it was possible to evaluate the content of K, Fe and Ni elements in the final product (encapsulated inorganic ion-exchanger): 0.8 mmol K g^{-1},

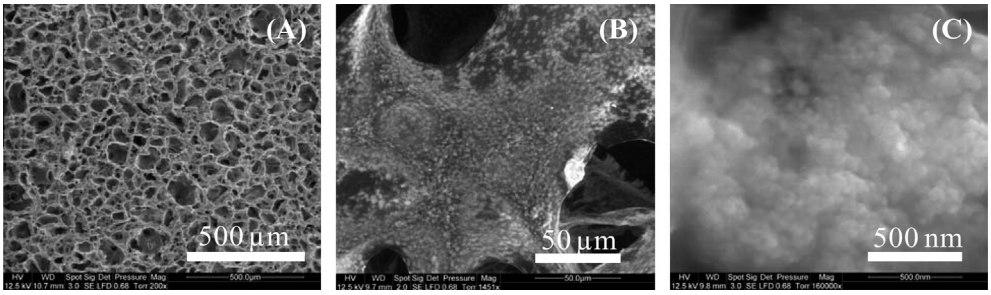

Fig. 1. Scanning electron micrograph of sorbent foams at different growing magnitudes.

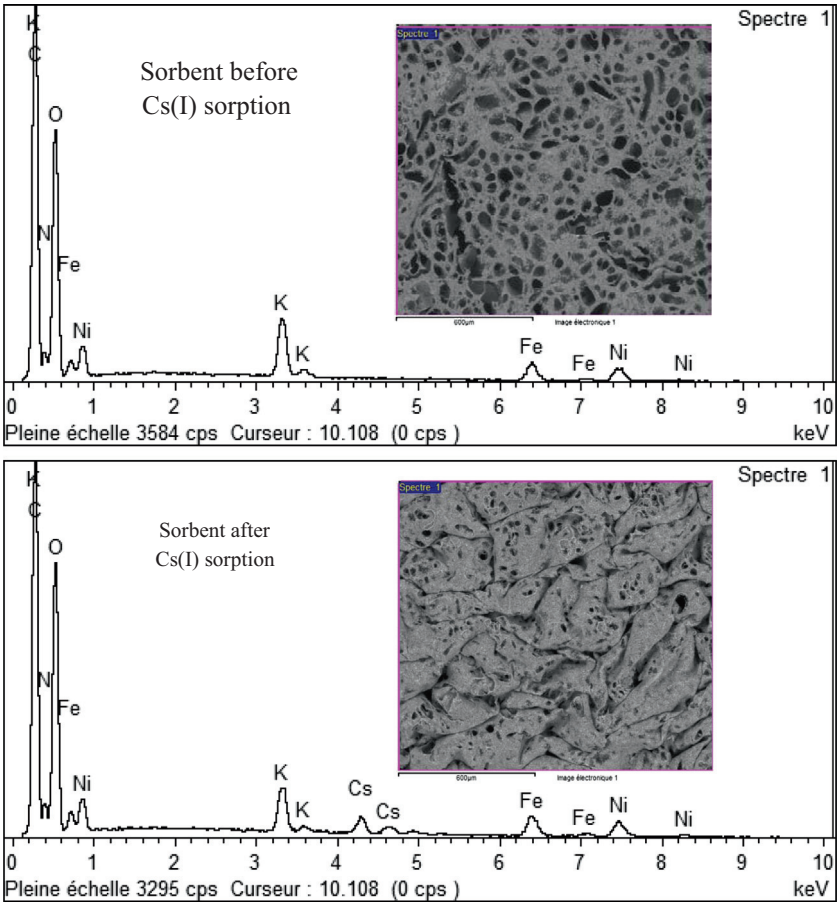

Fig. 2. SEM–EDX analysis of the sorbent before and after Cs(I) sorption (for element atomic quantification see Table 1).

Table 1
SEM–EDX analysis – Atomic quantification of elements (%, range on duplicate analysis).

Element (analytical line)	Before Cs(I) sorption	After Cs(I) sorption
C (K)	49.9–50.0	49.9–50.4
N (K)	13.0–13.2	13.6–13.8
O (K)	33.1–33.7	31.2–31.9
K (K)	1.40–1.41	1.05–1.16
Fe (K)	1.14–1.15	1.27–1.39
Ni(K)	1.46–1.49	1.53–1.76
Cs(L)	–	0.47–0.48

0.65 mmol Fe g^{-1} and 0.78 mmol Ni g^{-1}, respectively. The stoichiometry of the complex can be calculated to be $K_{1.2}Ni_{1.2}[Fe(CN)_6]$, based on their respective molar ratios (this means that about 33% of the sorbent is made of inorganic ion-exchanger). This is consistent with the semi-quantitative analysis performed by SEM–EDX analysis. This is obviously different than the expected value (for the theoretical pure salt; i.e., $K_2Ni[Fe(CN)_6]$). This probably means that the mineral sorbent immobilized in the foam is a mixture of different compounds including: $K_2Ni[Fe(CN)_6]$ and $Ni_2[Fe(CN)_6]$. This is also consistent with previous characterizations of the precipitates obtained by the reaction of nickel sulfate ($NiSO_4$) and potassium hexacyanoferrate ($K_4[Fe(CN)_6]$) [40]. XRay Diffraction analysis confirmed the impossibility to identify a pure complex (Fig. 3). The XRD pattern is characterized by three major peaks at positions 2θ: 17.59, 24.95, and 35.31–35.61. In addition, several peaks much lower have been detected at positions 2θ: 39.98–40.23, 43.92, 51.24, 54.48–54.60, and 60.7. The XRD pattern was compared to those of pure chemicals such as: $K_2Ni[Fe(CN)_6]\cdot 3H_2O$ (the reference of expected product), $Ni_2[Fe(CN)_6]\cdot xH_2O$, $Ni_{1.81}[Fe(CN)_6]\cdot 0.54H_2O$ and $Ni_2[Fe(CN)_6]\cdot 0.5H_2O$.

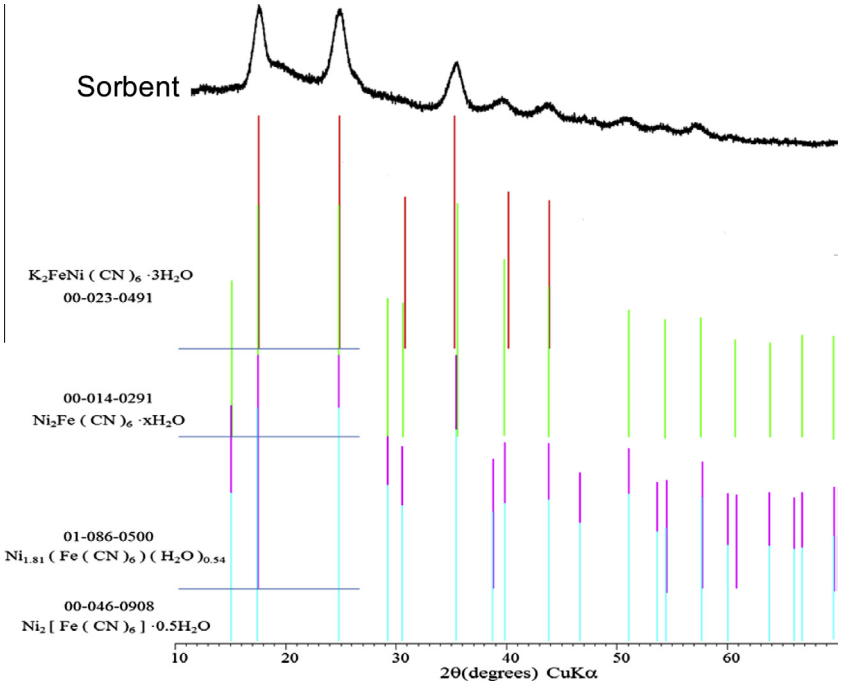

Fig. 3. XRD patterns of the hybrid inorganic ion-exchanger/chitin foam disc.

Though most of the peaks can be correlated to the presence of the expected nickel–potassium hexacyanoferrate, the presence of small peaks and the asymmetry of the broad peaks confirm that other products are present such as nickel ferrocyanide compounds (with different stoichiometry and different hydration). This could be explained by the presence of non-reacted reagents or sub-products of the synthesis. These peaks are very large due to the predominance of very small crystallites (classical effect for crystal sizes below 500 Å). Kołodyńska et al. [41] investigated nickel–potassium hexacyanoferrate (immobilized on magnetite composite matrix, prepared by polycondensation of sulfonated phenol and formaldehyde) for the binding of several anions. They compared the XRD diffraction patterns of the product with different ferrocyanide products (including $Ni_2[Fe(CN)_6]\cdot 6H_2O$, $K_2Ni[Fe(CN)_6]\cdot 1.5H_2O$, $KNi[Fe(CN)_6]$). Based on the element analysis (after solubilization and AAS analysis, 20.7% Ni(II), 14.8% Fe and 2.5% K(I), in mass) and the XRD patterns, they suggested that the material was formed of 60% of $K_2Ni[Fe(CN)_6]\cdot 1.5H_2O$, 35% of $Ni_2[Fe(CN)_6]$,$6H_2O$, and 5% of $KNi[Fe(CN)_6]$).

Based on the potassium content in the material (and assuming that all K(I) cations are exchangeable with Cs(I)) the maximum sorption capacity of the material should be close to 106 mg Cs g^{-1}.

3.2. Effect of pH on Cs(I) sorption

Fig. 4 reports the influence of pH on Cs(I) sorption using the hybrid discs. The pH was initially set between 1 and 9, after sorption the equilibrium was significantly changed. At initial pH 5.6 the final pH slightly increased to 5.8. For lower initial pHs, the final pH was shifted to higher pH values (by 0.8–0.9 unit), while for higher pH values the final pH tended to decrease by 1.6 unit (at pH 7.8) and up to 3.1 unit (at pH 9.5). So the system is very sensitive in terms of pH variations. However, the figure shows that the sorption capacity did not change at all for equilibrium pH ranging between 2.5 and 6.4: the sorption capacity under selected experimental conditions was 80.7 ± 0.7 mg Cs g^{-1}. This means that despite the pH variation the sorbent system is notably stable in terms of sorption capacity. This is consistent with the expected

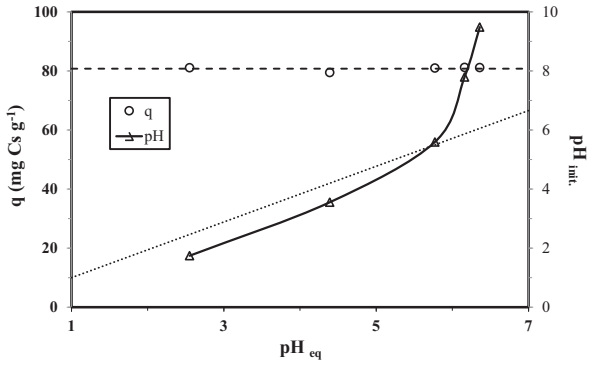

Fig. 4. pH effect on Cs(I) sorption (and pH variation during Cs(I) sorption) (C_0: 215 mg Cs L^{-1}; Sorbent dosage, SD: 2 g L^{-1}; alternate line shows the average value of sorption capacity, dot line shows the constant pH line).

ion exchange mechanism that occurs between K(I) and Cs(I) without any contribution of protons in the exchange process. Mimura et al. [42] also concluded that Cs(I) sorption (distribution coefficient) using potassium nickel hexacyanoferrate is hardly affected by the pH between 1 and 9. This is consistent with other studies using the same ion-exchanger: sorption efficiency slightly increased with pH [43]. Ishfaq et al. [1] reported that acid concentration does not interfere (up to 8 M concentrations) on Cs(I) sorption using potassium copper nickel hexacyanoferrate using hydrochloric acid and nitric acid while a significant decrease in sorption occurred in the case of sulfuric acid solutions: they attributed this decrease in sorption to a chemical degradation of the ion-exchanger.

3.3. Effect of competitor ions on Cs(I) sorption

Ion exchange mechanisms may be substantially influenced by the ionic strength of the solution and the presence of competitor ions. In order to verify the selectivity of the sorbent for Cs(I) a series of experiments was performed with increasing concentrations of competitor cations including Na(I), K(I), Rb(I) and NH_4^+. Fig. 5

shows that Cs(I) sorption capacity was hardly changed by the presence of Na(I) even at concentration as high as 1 M: the sorption capacity was 68.7 ± 6.8 mg Cs g^{-1} (in the 0–1 M Na(I) concentration range). For Rb(I) (in the range 0.01–0.5 M) Cs(I) sorption capacity randomly varied around 62.7 ± 2.8 mg Cs g^{-1}. For ammonium ions (in the range 0.01–0.5 M) Cs(I) sorption capacity varied (without clear trend) around 52.8 ± 3.4 mg Cs g^{-1}. All these experiments were performed with initial cesium concentrations of 135 mg Cs L^{-1} (with the same sorbent dosage; i.e., 2 g L^{-1}). The increasing amounts of competitor ions did not significantly change the sorption capacity for Cs(I) around slightly different levels that were controlled by different equilibrium pH values (pH_{eq}: 7.4 ± 0.2; 5.8 ± 0.1; 6.1 ± 0.2 for Na(I), Rb(I) and NH_4^+, respectively). For K(I) (concentration varying between 0.01 M and 0.1 M) experiments were performed with an initial Cs(I) concentration of 100 mg Cs L^{-1}: the sorption capacities were thus lower than for the other competitor ions (around 51.4 ± 4.1 mg Cs g^{-1}) and the equilibrium pH value varied around 6.8 ± 0.1. Table 2 compares the sorption efficiency for the different systems. These results confirm the analysis derived from Fig. 5: the addition of increasing amounts of competitor ions hardly changed the sorption efficiency for sorption. Under comparable concentration of Cs(I) (i.e., 135 mg Cs L^{-1}) the competitor effect can be ranked according to Na(I) < Rb(I) < NH_4^+. Mimura et al. [42] commented on the selectivity of potassium nickel hexacyanoferrate according Cs(I) > Rb(I) < NH_4^+ >> K(I) > Na(I) in agreement with the size of hydrated ions. Potassium competitive experiments (performed at 100 mg Cs L^{-1} initial concentrations) showed quite efficient Cs(I) sorption (above 95%). In the case of potassium copper nickel hexacyanoferrate ion-exchanger Cs(I) sorption was selective in the presence of concentrations as high as 8 M in $NaNO_3$ or KNO_3, while ammonium nitrate significantly reduced the distribution coefficient when the concentration exceeded 0.5 M [1].

These experiments clearly confirmed the results found in the literature that concluded that nickel potassium hexacyanoferrate ion-exchanger is selective to Cs(I). This is due to the crystalline structure of the ion-exchanger [42]. The face cubic centered structure contributes to give to the sorbent a narrow channel shape that allows the material to behave as an ion-sieving system for separating Cs(I) from larger hydrated cations [42].

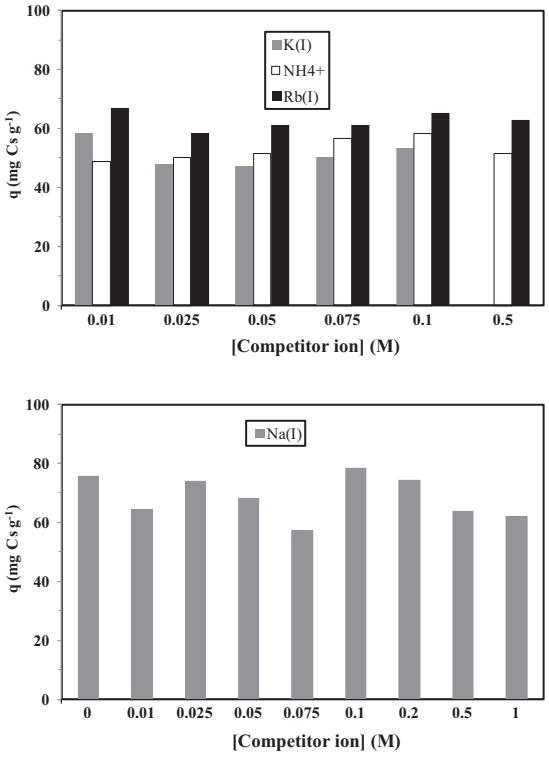

Fig. 5. Effect of competitor ions (K(I), Na(I), NH_4^+ and Rb(I)) on Cs(I) sorption (SD: 2 g L^{-1}; pH_{init}: 7–7.4; C_0: 100 mg Cs L^{-1} for K(I), and 135 mg Cs L^{-1} for Na(I), NH_4^+ and Rb(I)).

Table 2
Effect of competitor ions on Cs(I) sorption efficiency.

Competitor ion (M)	Na (I) (135 mg Cs L^{-1})	K(I) (100 mg Cs L^{-1})	NH_4^+ (135 mg Cs L^{-1})	Rb(I) (135 mg Cs L^{-1})
0	88.1	–	–	–
0.01	92.0	93.2	75.8	88.5
0.025	86.9	98.1	75.0	87.2
0.05	94.6	98.0	61.1	83.3
0.075	86.6	95.8	66.8	84.1
0.1	83.7	96.0	72.2	76.4
0.2	88.1	–	–	–
0.5	84.1	–	72.9	65.1
1	89.3	–	–	–
Average	88.2	96.2	70.6	80.8
St. dev.	3.3	1.8	5.2	8.0

3.4. Uptake kinetics

The original system developed in this study (consisting in the elaboration of filtration discs) requires a specific analysis of uptake kinetics taking into account the necessity to force the circulation of the solution through the highly porous structure. The interconnectivity of the holes and pores (heterogeneous in size) needs to improve the flow rate of recirculation to force the solution to pass through all the channels (and to achieve access to all the regions of the disc). For this reason the kinetic profiles (evolution of the residual concentration in the reactor) were compared for different flow rates: 6 mL min^{-1}, 30 ml min^{-1} and 300 mL min^{-1} (corresponding to superficial velocities of 0.73 m h^{-1}, 3.67 m h^{-1} and 36.7 m h^{-1}, respectively). Fig. 6 compares the kinetic profiles for the different flow rates. The flow rate hardly affects the kinetic profile between 5 and 30 mL min^{-1} while increasing the flow rate to 300 mL min^{-1} substantially improved uptake kinetics. This is confirmed by the parameters of the pseudo-second order rate equation (PSORE) (Table 3).

Pseudo-second order rate equation (PSORE) [44]:

$$\frac{dq(t)}{dt} = k_2(q_{eq} - q(t))^2 \quad (1a)$$

and after integration:

$$q(t) = \frac{q_{eq}^2 k_2 t}{1 + q_{eq} k_2 t} \quad (1b)$$

After linearization:

$$\frac{t}{q(t)} = \frac{1}{k_2 q_{eq}^2} + \frac{1}{q_{eq}} t \quad (1c)$$

where q_{eq} (mg g^{-1}) is the sorption capacity at equilibrium (calculated value from experimental data), k_2 (g mg^{-1} min^{-1}) is the pseudo-second order rate constant.

The impact of flow rate on uptake kinetics (especially at high flow velocity) may thus be explained by two main reasons: (a) the external diffusional mass transfer resistance, and (b) the presence of air bubbles (which may limit the contact of the solution with reactive groups). Increasing the flow rate makes the Nerst–Planck layer becoming narrower (and increasing the mass transfer rate). In addition, increasing the flow inside the foam helps in forcing the hydrodynamic transfer of the solution in the whole mass of the foam (independently of the potentially poor interconnectivity between the pores of the foam by forced transfer). In the case of

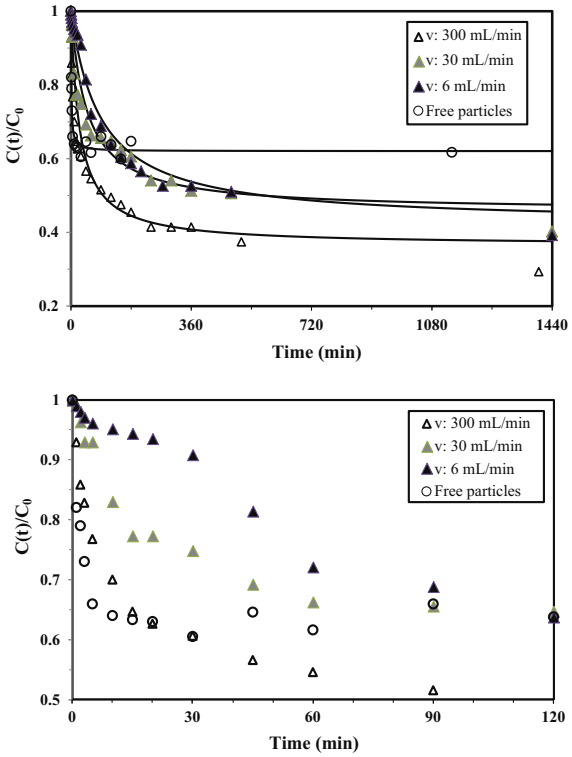

Fig. 6. Uptake kinetics – effect of recirculation flow rate on kinetic profiles and comparison with free inorganic ion-exchanger (C_0: 10 mg Cs L^{-1}; Sorbent dosage: 100 mg L^{-1}; pH 7; on the first panel the solid lines show the modeling of experimental data with the pseudo-second order rate equation using the parameters reported in Table 3).

Table 3
Cs(I) uptake kinetics – intrinsic (free particles) and apparent (foams) parameters of the Pseudo Second-Order Rate Equation (PSORE).

Sorbent	v (mL min^{-1})	q_{eq} (exp.) (mg Cs g^{-1})	q_{eq} (calc.) (mg Cs g^{-1})	k_2*10^4 (mg g^{-1} min^{-1})	R^2
FP	–	128.0	149.4	58.8	0.961
Foam	300	58.2	57.7	6.66	0.996
Foam	30	55.7	55.8	3.69	0.992
Foam	6	58.8	61.7	1.82	0.982

foam with small thickness of the walls of the scaffold intraparticle diffusion is not expected to play an important role. In addition it may be difficult accurately managing the thickness of scaffold walls. The impact of the size of different ferrocyanide particles (micro- and nano) is currently under investigation.

The sorption capacities at equilibrium are consistent between experimental values and calculated values; combined to the values of the correlation coefficient this means that the pseudo-second order rate equation fits well experimental data. Some discrepancies were observed in the case of FP (free ferrocyanide particles): the calculated value overestimated experimental values by about 17%. The sorption capacities are of the same order for the different flow rates: this was expected since the flow rate should just control the time to reach equilibrium and not the thermodynamics of the system. More interesting is the comparison of the kinetic coefficient (k_2): it continuously increased with increasing the flow rate. The uptake kinetics increases with the flow rate due to the improved accessibility of the solution to ion-exchanger particles immobilized in the foam: increasing the flow rate renews more frequently the solution at the surface of the sorbent improving the mass transfer. The direct comparison of the kinetic coefficients with free particles (without encapsulation) is not possible since the encapsulation contributes to improve the resistance to mass transfer. However, the difference in the k_2 values are large enough (about 15 times) to illustrate the impact of the immobilization process on mass transfer. It is interesting to compare the q_{eq} values. In the case of free particles, the sorption capacity is close to 128 mg Cs g^{-1}; this is much more than the levels reached with encapsulated materials (around 58 mg Cs g^{-1}). However, taking into account the amount of ion-exchanger in the resin (about 33% in the mixture chitosan/ion-exchanger precursors) the immobilized material shows a good efficiency/reactivity of the ion-exchanger. In addition the kinetic profile for the free particles showed a dispersion of the data at large contact time. When used as free particles the mixed Ni/K ferrocyanide particles appeared to be less stable compared to immobilized material (Cs(I) and/or microparticle release). Mimura et al. [42] investigated the kinetics of Cs(I) on potassium nickel hexacyanoferrate powder. They observed that the particle size influenced the mass transfer of Cs(I) on the inorganic ion-exchanger: increasing the size of the particles increased the time required to reach the equilibrium. However, the equilibrium concentration (and the sorption capacity) is not significantly affected; this means that the reactive groups remain accessible. Ismail et al. [43] reported a slight increase in the intraparticle diffusion coefficient when the size of the particle decreased. When immobilized on latex particles these ion-exchangers have very fast sorption kinetics: a few minutes are sufficient for reaching equilibrium [23]. The immobilization of the ion-exchanger on mushroom biomass (*Agaricus bisporus*) also allowed fast Cs(I) sorption kinetics (less than 30 min, with low metal concentrations and high sorbent dosage) [21]. The PSORE was used for evaluating the kinetic rate parameter (k_2) that was found to be close to 0.09 g µmol^{-1} min^{-1} (0.677 g mg^{-1} min^{-1}). This is 3 orders of magnitude higher than the values found for the present system. It is noteworthy that the concentration is much greater in this study compared to the study with *A. bisporus* support. It is thus difficult directly comparing the kinetic parameters.

3.5. Sorption isotherm

Sorption isotherm was obtained using the recirculation mode in static regime by contact of a disc (immobilized in a filtration membrane holder) with a fixed volume of Cs(I) solution at pH 7 and at increasing Cs(I) concentrations. Fig. 7 reports the sorption isotherm of Cs(I). The shape of the isotherm (q = f(Ceq), where q is the sorption capacity (mg Cs g^{-1}) and C_{eq} is the residual Cs concentration, mg Cs L^{-1}) is characterized by a saturation plateau (residual concentration above 100 mg Cs L^{-1}). This is a first indication that the Langmuir equation (which is characterized by an

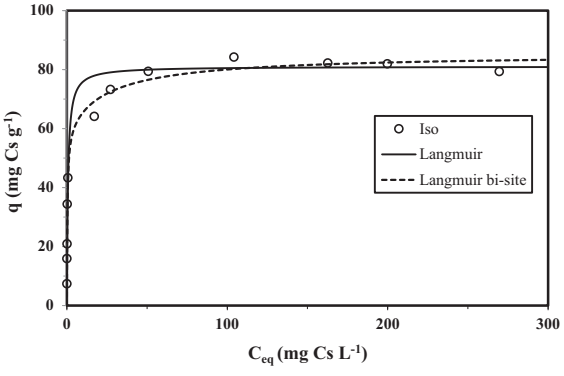

Fig. 7. Cs(I) sorption isotherm (pH 7; Solid curve shows the modeling of sorption isotherm using the Langmuir equation and dot line shows the modeling with the Langmuir bi-site equation).

asymptotic trend) will fit better experimental data than the Freundlich equation (which is described by a power-type equation: $q = k_F C_{eq}^{1/n}$, where k_F and $1/n$ are the parameters of the Freundlich equation). The solid line in Fig. 6 shows the simulation of sorption isotherm with the Langmuir equation:

$$q = q_m b C_{eq}/(1 + bC_{eq}) \quad (2)$$

where q_m (mg Cs g^{-1}) is the sorption capacity of the sorbent at saturation of the monolayer and b is the affinity coefficient (L mg^{-1}). Here the maximum sorption capacity is close to 81 mg Cs g^{-1} while the affinity coefficient is close to 1.46 L mg^{-1}. The inorganic ion-exchanger mass fraction in the sorbent is close to 33%. This means that the maximum sorption capacity is about 243 mg Cs g^{-1} (nickel–potassium ferrocyanide). This maximum sorption capacity is far below the values reached with free $K_2Ni[Fe(CN)_6]$ particles about 342 mg Cs g^{-1} (i.e., 2.57 mmol Cs g^{-1} at pH 7.5–9.3, consistently with K(I) content of the synthesized product, i.e., 2.58 mmol K g^{-1}) [42], and the values cited by Ishfaq et al. (2.33–2.58 mmol Cs g^{-1} at pH 2, [1]), and by Ismail et al. [43] (3.95 mmol Cs g^{-1} at pH 5.5, or 520 mg Cs g^{-1}). The inorganic ion-exchanger fraction in the material is assumed to be close to 0.8 mmol g^{-1} (based on potassium content); this means that the theoretical maximum exchange capacity is close to 106 mg Cs g^{-1}. The maximum sorption capacity is thus 20% less than the theoretical value. However, this sorption capacity is much higher than that found for $K_2Ni[Fe(CN)_6]$ immobilized on silica gels (19–41 mg Cs g^{-1}, [5]), on polymethacrylate support (20 mg Cs g^{-1}, [45]), on latex particles (3.5 mg Cs g^{-1}, [23]).

Fig. 7 shows that the plot overestimates the sorption capacity at intermediary section of the curve. A better fit of experimental data can be obtained using the Langmuir bi-site equation [46,47]. This behavior is typical of systems involving several types of sorption sites with different adsorption energy. The concept of bi-site Langmuir equation was first developed to take into account the heterogeneities of sorbents (presence of different groups with different affinity for target solute). Differences in energy adsorption may also result from changes in the metal species that are adsorbed on the sorbent. This makes the concept of bi-site Langmuir equation extendable to systems involving also the binding of different types of solute (including a solute present under different forms with different affinities for sorption sites). Assuming that several sites could be involved in the binding (or that several species could be bound with different affinity), the Langmuir equation becomes:

3.5.1. Langmuir bi-site equation

$$q = \frac{q_{m,1} b_1 C_{eq}}{1 + b_1 C_{eq}} + \frac{q_{m,2} b_2 C_{eq}}{1 + b_2 C_{eq}} = \frac{60.3 \times 3.08 C_{eq}}{1 + 3.08 C_{eq}} + \frac{25.0 \times 0.039 C_{eq}}{1 + 0.039 C_{eq}} \quad (3)$$

where ($q_{m,1}$, b_1) and ($q_{m,2}$, b_2) are the parameters for the two types of sorption sites.

The affinity coefficients (b_1 and b_2) are significantly different reflecting the differences in strength of the interaction of the solute with these different sorption sites (or different metal species). The fitted curve (using the bi-site model) is represented by dot line in Fig. 7.

The Freundlich equation was also used for fitting experimental data for the simulation of breakthrough curves using the Clark model (see below) and the parameters of the model were found to be: k = 5.12 and n = 7.58.

3.6. Cs(I) uptake in dynamic mode – Breakthrough curve

Fig. 8 shows the breakthrough obtained using 0.5 g hybrid discs (i.e., 5 disks) for the treatment of 8 L of Cs(I) solution (10 mg Cs L^{-1}). A first plateau was observed within the first 2 L passed through the column corresponding to an outlet concentration of less than 0.5 mg Cs L^{-1}. The saturation plateau was approached near to 7 L of solution. The slope of the breakthrough is not steep, meaning that resistance to mass transfer is controlling the uptake kinetics. The flow rate being 148 ml h^{-1}, this corresponds to a superficial flow velocity of 0.3 m h^{-1}. This is a low superficial flow velocity. Based on the results obtained in static mode, it appears that increasing the flow velocity would decrease the resistance to mass transfer (forcing the solution to access all reactive sites in the core of the foam). However, this would decrease the mean contact time. The solution would consist in re-circulating the solution through the column at high flow rate while the intermediary tank reactor would be fed with a constant flow of renewed solution. This process would combine the dynamic mode while maintaining the optimized contact of the solution with internal reactive groups into the foam discs.

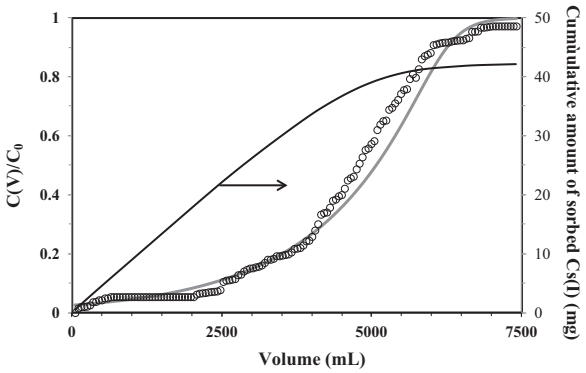

Fig. 8. Cs(I) sorption in dynamic mode (fixed bed column) – Breakthrough curve (C_0: 10 mg Cs L^{-1}; [$NaNO_3$]: 0.01 M; Amount of sorbent 500 mg; gray solid line shows the modeling of breakthrough curve with the model of Clark).

The cumulative amount of Cs sorbed on the discs is shown by the black solid line in Fig. 8. The corresponding sorption capacity at saturation is close to 84 mg Cs g^{-1}. This means that the sorption capacity is of the same order than the maximum sorption capacity obtained on sorption isotherms. This is slightly higher than the sorption capacity corresponding to a residual concentration of 10 mg Cs L^{-1} on the sorption isotherm curve.

The breakthrough curve was simulated using the Clark model. Though this model was initially developed for systems obeying to the Freundlich equation (for the description of sorption isotherm and metal distribution between the aqueous and solid phases) in the present case with the initial concentration set to 10 mg Cs L^{-1} the sorption isotherm remains in the initial linear part of the curve where both the Freundlich and the Langmuir equation would both fit well sorption isotherm. The mass transfer in the column is described by the following equation [49]:

$$C_{out}/C_{in} = [1/(1 + Ae^{-rt})]^{1/n-1} \quad (4a)$$

$$\text{with} \quad A = [(C_{in}^{n-1}/C_b n - 1) - 1]e^{rt} b \quad (4b)$$

where C_{in} and C_{out} are the inlet and outlet concentrations (mg Cs L^{-1}), respectively. C_b is the breakthrough concentration (arbitrary set, mg Cs L^{-1})) corresponding to the breakthrough time (t_b), n is the Freundlich exponent, and r is the rate coefficient (min^{-1}). The simulated curve (obtained from the Clark equation, gray solid curve in Fig. 8) fits well experimental data (Fig. 8) using the values of the parameters: (a) r: 0.0095 min^{-1}, and (b) ln$A$: 24.05.

3.7. Stability of the sorbent

The stability of the sorbent and the stability of Cs(I) on the sorbent can be evaluated through two types of criteria: (a) release

Table 4
Cs(I) sorption from ^{137}Cs-spiked solutions.

^{137}Cs		Stable Cs		Performance parameters		
A_0 (Bq L^{-1})	A_f (Bq L^{-1})	C_0 (mmol L^{-1})	C_f (mmol L^{-1})	DF (A_0/A_f)	q (mmol g^{-1})	K_d (L g^{-1})
41,000	135	4.0×10^{-5}	1.3×10^{-7}	304	2.12×10^{-5}	164
41,000	73	2.0×10^{-3}	3.6×10^{-6}	562	1.08×10^{-3}	300
41,000	55	2.0×10^{-2}	2.7×10^{-5}	745	1.17×10^{-2}	433

A: activity of solution (^{137}Cs); C: Cs total concentration; DF: decontamination factor; q: sorption capacity (cumulative); K_d (distribution coefficient: q/C_f).

of Ni(II) and Fe(II,III) in the solution during Cs(I) sorption, and (b) ready desorption using 1 M KCl solution. The stability of the ion-exchanger was investigated by the analysis of Ni(II) and Fe(II,III) in the outlet of the column (after passing about 8 L of Cs(I) solution). The mass balance showed that less than 1.1% of iron present on the fixed bed was released from the column while nickel was almost no detectable. The desorption of Cs(I) from loaded sorbent was investigated on the samples collected from the sorption isotherms. These samples were contacted with 5 mL of 1 M KCl solutions at very low flow rate (2 days, continuous flow) and the elution treatment was repeated in order to evaluate the percentage of Cs(I) released. The first desorption removed about 14% of sorbed cesium, while the second desorption step removed about 4% of the metal. These experiments show a good stability of the ion-exchanger in the biopolymer matrix and a good stability of bound Cs(I). This is important for the evaluation of these materials for Cs(I) entrapment and confinement.

3.8. ^{137}Cs sorption in static mode

The preliminary tests performed on ^{137}Cs-spiked solutions are summarized in Table 4. The residual concentration of Cs was calculated based on the analysis of ^{137}Cs activity (A) (mass balance and removal yield). The sorption capacity was calculated at each step and the cumulative sorption capacity was evaluated at each step (appearing in Table 4). Both the decontamination factor (DF: A_0/A_f, equivalent to C_0/C_f)) and the distribution coefficient (K_d: q/C_f) are increasing with the amount of Cs. The increase of the K_d with metal concentration was expected since the increase of the concentration results in a strong increase in sorption capacity. The increase of the DF is probably due to a better efficiency of the system due to the progressive hydration of the discs that improves the accessibility to reactive groups. In addition, the first minutes or hours of operation lead to a progressive washing of the few particles of inorganic ion exchanger that are not tightly bound to the biopolymer, resulting in a possible partial release of Cs ions due to their association with released ion exchanger particles. An efficient washing/conditioning of the discs prior to contact with metal solution, associated with an efficient pre-hydration of the disc would significantly improve the initial DF. Under selected experimental conditions (low concentrations below 0.2 mmol L^{-1}; i.e., below 2.3 mg Cs L^{-1}) the sorption capacity linearly increased with residual concentration (Henry's type isotherm). The sorption capacity reached a value of 1.6 mg Cs g^{-1} for a residual concentration of Cs of 3.5 μg L^{-1}. The sorption yield (measured by the activity of the solutions) confirms the high efficiency of the sorbent for recovering ^{137}Cs: sorption efficiency exceeded 99.7% under selected experimental conditions.

4. Conclusion

Potassium-nickel hexacyanoferrate immobilized in chitin matrix (conditioned under the form of highly porous discs) can be used for the reactive filtration of cesium solutions. The XRD analysis (mixture of amorphous and crystalline structures), and the SEM–EDX analysis confirmed the results of element analysis (performed on mineralized sorbent using sulfuric acid and hydrogen peroxide for material degradation): the $K_{1.2}Ni_{1.2}[Fe(CN)_6]$) ion-exchanger is constituted of a mixture of $K_2Ni[Fe(CN)_6]$ and $Ni[Fe(CN)_6]$. The sorption appears to be independent of the pH (at least in the range 2.5-6.4). The presence of competitor cations such as Na(I), Rb(I) or K(I) hardly influenced Cs(I) sorption. Sorption isotherm is described by the Langmuir equation and maximum sorption capacity reaches up to 81 mg Cs g^{-1}. This is lower (by about 20%) than the theoretical sorption capacity expected from K(I) content. The uptake kinetics is considerably decreased compared to the kinetic profiles obtained with free ion-exchanger particles. However, when the flow rate (with recirculation) is increased the mass transfer is significantly improved and the apparent rate coefficient (determined by the pseudo-second order rate equation) also increased. The stability of the sorbent demonstrated by (a) the weak release of nickel and Fe during Cs(I) sorption, and (b) the stability of Cs(I) during KCl elution confirm the strength of the interaction of Cs(I) with the inorganic ion-exchanger (especially when immobilized in chitin matrix). The breakthrough curve (obtained from fixed-bed column experiment) shows the efficiency of the system for reactive filtration of Cs(I)-containing solutions. Finally, the system was tested with ^{137}Cs-spiked solutions (41 kBq L^{-1}) and a maximum distribution coefficient close to 433 L g^{-1} was obtained.

Acknowledgments

Authors thank Jean-Marie Taulemesse and Gwenn Le Saout from Centre des Matériaux des Mines d'Alès (EMA) for SEM/SEM–EDX analysis and XRD analysis, respectively.

References

[1] M.M. Ishfaq, H.M.A. Karim, M.A. Khan, Adsorption studies of cesium on potassium copper-nickel hexacyanoferrate(II) from aqueous solutions, J. Radioanal. Nucl. Chem. 170 (2) (1993) 321.

[2] M.M. Ishfaq, H.M.A. Karim, M.A. Khan, A radiochemical study on the thermodynamics of cesium adsorption on potassium copper nickel hexacyanoferrate(II) from aqueous solutions, J. Radioanal. Nucl. Chem. 222 (1–2) (1997) 177.

[3] I. Ismail, M. El-Sourougy, N. Moneim, H. Aly, Preparation, characterization, and utilization of potassium nickel hexacyanoferrate for the separation of cesium and cobalt from contaminated waste water, J. Radioanal. Nucl. Chem. 237 (1) (1998) 97.

[4] H. Mimura, M. Kimura, K. Akiba, Y. Onodera, Selective removal of cesium from sodium nitrate solutions by potassium nickel hexacyanoferrate-loaded chabazites, Sep. Sci. Technol. 34 (1) (1999) 17.

[5] H. Mimura, M. Kimura, K. Akiba, Y. Onodera, Selective removal of cesium from highly concentrated sodium nitrate neutral solutions by potassium nickel hexacyanoferrate(II)-loaded silica gels, Solvent Extr. Ion Exch. 17 (2) (1999) 403.

[6] F. Han, G.-H. Zhang, P. Gu, Removal of cesium from simulated liquid waste with countercurrent two-stage adsorption followed by microfiltration, J. Hazard. Mater 225-226 (2012) 107.

[7] C. Loos-Neskovic, S. Ayrault, V. Badillo, B. Jimenez, E. Garnier, M. Fedoroff, D.J. Jones, B. Merinov, Structure of copper-potassium hexacyanoferrate (II) and sorption mechanisms of cesium, J. Solid State Chem. 177 (6) (2004) 1817.

[8] P.J. Faustino, Y. Yang, J.J. Progar, C.R. Brownell, N. Sadrieh, J.C. May, E. Leutzinger, D.A. Place, E.P. Duffy, F. Houn, S.A. Loewke, V.J. Mecozzi, C.D. Ellison, M.A. Khan, A.S. Hussain, R.C. Lyon, Quantitative determination of cesium binding to ferric hexacyanoferrate: Prussian blue, J. Pharm. Biomed. Anal. 47 (1) (2008) 114.

[9] N.Y. Kremlyakova, V.M. Komarevsky, Sorption of alkaline and alkaline-earth radionuclides on zirconium phosphate sorbent Termoxid-3A from aqueous solutions, J. Radioanal. Nucl. Chem. 218 (2) (1997) 197.
[10] V.N. Lebedev, N.A. Mel'nik, A.V. Rudenko, Sorption of cesium on titanium and zirconium phosphates, Radiochemistry 45 (2) (2003) 149.
[11] G.S. Murthy, M.V. Sivaiah, S.S. Kumar, V.N. Reddy, R.M. Krishna, S. Lakshminarayana, Adsorption of cesium on a composite inorganic exchanger zirconium phosphate – ammonium molybdophosphate, J. Radioanal. Nucl. Chem. 260 (1) (2004) 109.
[12] E.I. Shabana, M.I. El-Dessouky, Sorption of cesium and strontium ions on hydrous titanium dioxide from chloride medium, J. Radioanal. Nucl. Chem. 253 (2) (2002) 281.
[13] S. Gaur, Determination of Cs-137 in environmental water by ion-exchange chromatography, J. Chromatogr., A 733 (1–2) (1996) 57.
[14] C.-Y. Chang, L.-K. Chau, W.-P. Hu, C.-Y. Wang, J.-H. Liao, Nickel hexacyanoferrate multilayers on functionalized mesoporous silica supports for selective sorption and sensing of cesium, Microporous Mesoporous Mater. 109 (1–3) (2008) 505.
[15] J. Orechovska, P. Rajec, Sorption of cesium on composite sorbents based on nickel ferrocyanide, J. Radioanal. Nucl. Chem. 242 (2) (1999) 387.
[16] P. Rajec, J. Orechovska, I. Novak, NIFSIL: a new composite sorbent for cesium, J. Radioanal. Nucl. Chem. 245 (2) (2000) 317.
[17] A. Voronina, V. Semenishchev, E. Nogovitsyna, N. Betenekov, A study of ferrocyanide sorbents on hydrated titanium dioxide support using physicochemical methods, Radiochemistry 54 (1) (2012) 69.
[18] V. Milyutin, O. Kononenko, S. Mikheev, V. Gelis, Sorption of cesium on finely dispersed composite ferrocyanide sorbents, Radiochemistry 52 (3) (2010) 281.
[19] I. Sheveleva, V. Avramenko, S. Bratskaya, V. Zheleznov, E. Modin, V. Sergienko, Composite sorbents for recovery of cesium radionuclides, Russ. J. Appl. Chem. 83 (12) (2010) 2115.
[20] I. Sheveleva, V. Zheleznov, S. Bratskaya, V. Avramenko, V. Kuryavyi, Sorption of cesium radionuclides with composite carbon fibrous materials, Russ. J. Appl. Chem. 84 (7) (2011) 1152.
[21] J. Vrtoch, M. Pipíška, M. Horník, J. Augustín, J. Lesný, Sorption of cesium from water solutions on potassium nickel hexacyanoferrate-modified *Agaricus bisporus*; mushroom biomass, J. Radioanal. Nucl. Chem. 287 (3)(2011) 853.
[22] T.J. Tranter, R.S. Herbst, T.A. Todd, A.L. Olson, H.B. Eldredge, Evaluation of ammonium molybdophosphate-polyacrylonitrile (AMP-PAN) as a cesium selective sorbent for the removal of Cs-137 from acidic nuclear waste solutions, Adv. Environ. Res. 6 (2) (2002) 107.
[23] V. Avramenko, S. Bratskaya, V. Zheleznov, I. Sheveleva, O. Voitenko, V. Sergienko, Colloid stable sorbents for cesium removal: preparation and application of latex particles functionalized with transition metals ferrocyanides, J. Hazard. Mater. 186 (2–3) (2011) 1343.
[24] A. Iwanade, N. Kasai, H. Hoshina, Y. Ueki, S. Saiki, N. Seko, Hybrid grafted ion exchanger for decontamination of radioactive cesium in Fukushima Prefecture and other contaminated areas. J. Radioanal. Nucl. Chem. 1 (2012).
[25] A. Nilchi, R. Saberi, M. Moradi, H. Azizpour, R. Zarghami, Evaluation of AMP–PAN composite for adsorption of Cs^+ ions from aqueous solution using batch and fixed bed operations, J. Radioanal. Nucl. Chem. 292 (2)(2012) 609.
[26] X.S. Ye, Z.J. Wu, W. Li, H.N. Liu, Q. Li, B.J. Qing, M. Guo, F. Go, Rubidium and cesium ion adsorption by an ammonium molybdophosphate-calcium alginate composite adsorbent, Colloids Surf., A 342 (1–3) (2009) 76.
[27] S. Sarkar, E. Guibal, F. Quignard, A. SenGupta, Polymer-supported metals and metal oxide nanoparticles: synthesis, characterization, and applications, J. Nanopart. Res. 14 (2) (2012) 1.
[28] H. Mimura, M. Saito, K. Akiba, Y. Onodera, Selective uptake of cesium by ammonium molybdophosphate (AMP)–calcium alginate composites, J. Nucl. Sci. Technol. 38 (10) (2001) 872.
[29] H. Mimura, W. Yan, Y. Wang, Y. Niibori, I. Yamagishi, M. Ozawa, T. Ohnishi, S. Koyama, Selective separation and recovery of cesium by ammonium tungstophosphate-alginate microcapsules, Nucl. Eng. Des. 241 (12) (2011) 4750.
[30] E. Rumyantseva, A. Veleshko, S. Kulyukhin, I. Veleshko, D. Shaitura, K. Rozanov, N. Dmitrieva, Preparation and properties of modified spherically granulated chitosan for sorption of ^{137}Cs from solutions, Radiochemistry 51 (5) (2009) 496.
[31] P. Krys, F. Testa, A. Trochimczuck, C. Pin, J.M. Taulemesse, T. Vincent, E. Guibal, Encapsulation of ammonium molybdophosphate and zirconium phosphate in alginate matrix for the sorption of rubidium(I), J. Colloid Interface Sci. 409 (2013) 141.
[32] H. Mimura, H. Ohta, K. Akiba, Y. Onodera, Selective uptake and recovery of palladium by biopolymer microcapsules enclosing Cyanex 302 extractant, J. Nucl. Sci. Technol. 38 (5) (2001) 342.
[33] Y. Wu, M. Outokesh, H. Mimura, Y. Niibori, Selective uptake properties of metal ions by hybrid microcapsules enclosed with TBP, Prog. Nucl. Energy 50 (2–6) (2008) 487.
[34] E. Guibal, T. Vincent, C. Jouannin, Immobilization of extractants in biopolymer capsules for the synthesis of new resins: a focus on the encapsulation of tetraalkyl phosphonium ionic liquids, J. Mater. Chem. 19 (45) (2009) 8515.
[35] K. Campos, R. Domingo, T. Vincent, M. Ruiz, A.M. Sastre, E. Guibal, Bismuth recovery from acidic solutions using Cyphos IL-101 immobilized in a composite biopolymer matrix, Water Res. 42 (14) (2008) 4019.
[36] C. Jouannin, I. Dez, A.-C. Gaumont, J.-M. Taulemesse, T. Vincent, E. Guibal, Palladium supported on alginate/ionic liquid highly porous monoliths: application to 4-nitroaniline hydrogenation, Appl. Catal., B 103 (3–4) (2011) 445.
[37] T. Vincent, P. Krys, C. Jouannin, A.-C. Gaumont, I. Dez, E. Guibal, Hybrid macroporous Pd catalytic discs for nitrotoluene hydrogenation: contribution of the alginate-alkylphosphonium ionic liquid support, J. Organomet. Chem. 723 (1) (2013) 90.
[38] C. Jouannin, C. Vincent, I. Dez, A.-C. Gaumont, T. Vincent, E. Guibal, Highly porous catalytic materials with Pd and ionic liquid supported on chitosan, J. Appl. Polym. Sci. 128 (5) (2013) 3122.
[39] Y. Barré, Etude des ferrocyanures de nickel et de cobalt en vue de la maîtrise des rejets de nickel, Rapport CEA, 2005.
[40] D. Kołodyńska, Z. Hubicki, B. Kubica, Hexacyanoferrate composite sorbent in removal of anionic species from waters and waste waters, Sep. Sci. Technol. 47 (9) (2012) 1361.
[41] H. Mimura, J. Lehto, R. Harjula, Ion exchange of cesium on potassium nickel hexacyanoferrate(II)s, J. Nucl. Sci. Technol. 34 (5) (1997) 484.
[42] I.M. Ismail, M.R. El-Sourougy, N. Abdel Moneim, H.F. Aly, Equilibrium and kinetic studies of the sorption of cesium by potassium nickel hexacyanoferrate complex, J. Radioanal. Nucl. Chem. 240 (1) (1999) 59.
[43] Y.S. Ho, Second-order kinetic model for the sorption of cadmium onto tree fern: a comparison of linear and non-linear methods, Water Res. 40 (1) (2006) 119.
[44] S. Taj, D. Muhammad, M.A. Chaudhry, M. Mazhar, Lithium, rubidium and cesium ion removal using potassium iron(III) hexacyanoferrate(II) supported on polymethylmethacrylate, J. Radioanal. Nucl. Chem. 288 (1) (2011) 79.
[45] R.R. Escudero, M. Robitzer, F. Di Renzo, F. Quignard, Alginate aerogels as adsorbents of polar molecules from liquid hydrocarbons: hexanol as probe molecule, Carbohydr. Polym. 75 (1) (2009) 52.
[46] A. Butewicz, K.C. Gavilan, A.V. Pestov, Y. Yatluk, A.W. Trochimczuk, E. Guibal, Palladium and platinum sorption on a thiocarbamoyl-derivative of chitosan, J. Appl. Polym. Sci. 116 (6) (2010) 3318.
[47] T. Vincent, J.M. Taulemesse, A. Dauvergne, T. Chanut, F. Testa, E. Guibal, Thallium(I) sorption using prussian blue immobilized in alginate capsules, Carbohydr. Polym. 99 (2014) 517.
[48] R.M. Clark, Evaluating the cost and performance of field-scale granular activated carbon systems, Environ. Sci. Technol. 21 (1987) 573.